

Ripples and dots generated by lattice gases

Géza Ódor (1), Bartosz Liedke, Karl-Heinz Heinig, and Jeffrey Kelling (2)

(1) *Research Institute for Technical Physics and Materials Science, P.O.Box 49, H-1525 Budapest, Hungary*

(2) *Institute of Ion Beam Physics and Materials Research Helmholtz-Zentrum Dresden-Rossendorf P.O.Box 51 01 19, 01314 Dresden, Germany*

Abstract

We show that the emergence of different surface patterns (ripples, dots) can be well understood by a suitable mapping onto the simplest nonequilibrium lattice gases and cellular automata. Using this efficient approach difficult, unanswered questions of surface growth and its scaling can be studied. The mapping onto binary variables facilitates effective simulations and enables one to consider very large system sizes. We have confirmed that the fundamental Kardar-Parisi-Zhang (KPZ) universality class is stable against a competing roughening diffusion, while a strong smoothing diffusion leads to logarithmic growth, a mean-field type behavior in two dimensions. The model can also describe anisotropic surface diffusion processes effectively. By analyzing the time-dependent structure factor we give numerical estimates for the wavelength coarsening behavior.

1. Introduction

In nanotechnologies, patterns of large areas are to be assembled in a cost effective way, possibly by self-organization processes. Different materials under different conditions have been shown to exhibit dot and ripple formation in a rather universal manner [1]. Universality appears, when microscopic details of interactions become irrelevant, i.e. the diverging correlation length and the complex behavior of the system dominates. This is typical in nonequilibrium systems with currents [2, 3]. It was pointed out [4, 5] that grooved surfaces and growth instabilities may emerge as the consequence of broken detailed balance condition

$$P(C)R_{C \rightarrow C'} \neq P(C')R_{C' \rightarrow C} \quad (1)$$

where $P(C)$ denotes the probability of the state C and $R_{C \rightarrow C'}$ is the transition rate between states C and C' . This means that complex structures and patterns can emerge during relaxation in nonequilibrium system. In case of ion-beam-induced modification of surfaces the first theory to explain pattern formation was suggested long time ago [6].

To demonstrate the general tendency of self-organization we present here simple case studies of fundamental models of statistical physics, showing

universal scaling and pattern formation. Understanding of basic surface growth models still lacks many details, although the basic universality classes and important models have been introduced [7, 8]. Analytical tools like continuum field methods have limited applicability, while numerical simulations have achieved limited precision.

One of the simplest nonlinear stochastic differential equation set up by Kardar, Parisi and Zhang (KPZ) [9] describes the dynamics of surface growth processes in the thermodynamic limit. It specifies the evolution of the height function $h(\mathbf{x}, t)$ in the d -dimensional space

$$\partial_t h(\mathbf{x}, t) = v + \sigma \nabla^2 h(\mathbf{x}, t) + \lambda (\nabla h(\mathbf{x}, t))^2 + \eta(\mathbf{x}, t) . \quad (2)$$

Here v and λ are the amplitudes of the mean and local growth velocity, σ can be understood as a coefficient of surface tension driven smoothing and η roughens the surface by a zero-average, Gaussian noise field exhibiting the variance: $\langle \eta(\mathbf{x}, t) \eta(\mathbf{x}', t') \rangle = 2D \delta^d(\mathbf{x} - \mathbf{x}') (t - t')$. The notation D is used for the noise amplitude and $\langle \rangle$ means the distribution average. The surface scaling exponents are known in $(1+1)d$ [10], but for the case considered here, 2-dimensional surfaces of 3-dimensional system, as well as in higher dimensions approximations are available only. The exis-

tence of a finite upper critical dimension, where a smooth mean-field behavior would enter is also debated. As the result of the competition of roughening and smoothing terms, models described by the KPZ equation exhibit a roughening phase transition between a weak-coupling regime ($\lambda < \lambda_c$), governed by the Edwards-Wilkinson (EW) fixed point at $\lambda = 0$ [11], and a strong coupling phase. The strong coupling fixed point is inaccessible by the perturbative renormalization group method. Therefore, the KPZ phase space has been the subject of controversies for a long time.

Mapping of surface growth onto reaction-diffusion system allows effective numerical simulations and understanding of basic universality classes [12, 13]. In one dimension a discrete, restricted solid on solid (RSOS) realization of the KPZ growth is equivalent to the Asymmetric Simple Exclusion Process of particles [14], while some of us have shown that the roof-top model mapping [15, 16] can be generalized to higher dimensions [17, 18].

In two dimensions one can map KPZ processes onto anisotropic, but oriented migration of directed dimers [17]. This mapping is interesting not conceptually only, linking nonequilibrium surface growth with the dynamics of driven lattice gases [2, 19], but provides an efficient tool for investigating debated and unresolved problems numerically [18]. The surface built up from the octahedra can be represented by the edges meeting in the up/down middle vertexes (see Fig. 1). The up edges in the $\chi = x$ or $\chi = y$ directions at the lattice site i, j are represented by $\sigma_\chi(i, j) = +1$, while the down ones by $\sigma_\chi(i, j) = -1$ slopes of the model. In this way an octahedron site deposition flips four edges, meaning two '+1' \leftrightarrow '-1' exchanges: one in the x and one in the y direction. This can be described by the generalized update rule:

$$\begin{pmatrix} -1 & 1 \\ -1 & 1 \end{pmatrix} \xrightarrow[\frac{q}{p}]{} \begin{pmatrix} 1 & -1 \\ 1 & -1 \end{pmatrix} \quad (3)$$

with probability p for attachment and probability q for detachment. We can also call '+1'-s as particles and '-1'-s as holes of a reaction-diffusion model on a square lattice. Thus, an attachment/detachment update corresponds to a single step motion of an oriented dimer in the bisectrix direction of the x and y axes. We update the neighborhood of the sub-lattice points, which are the crossing-points of the dashed lines. In [17, 18] we derived how this mapping connects the microscopic model to the KPZ equation with $\lambda = 2\frac{p}{p+q} - 1$ and investigated its

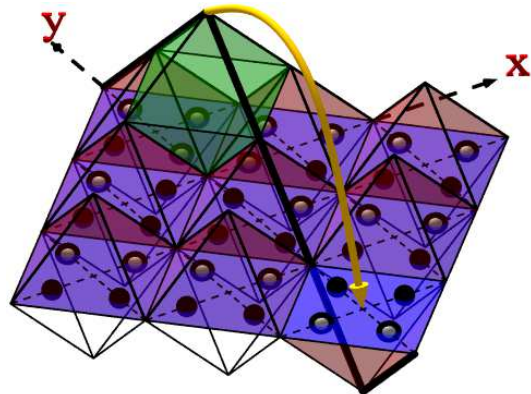


Figure 1: Mapping of the 2 + 1 dimensional surface growth onto the 2d particle model (bullets). Surface attachment (with probability p) and detachment (with probability q) corresponds to exchanges of particles, or to anisotropic diffusion of dimers in the bisectrix direction of the x and y axes. The crossing points of dashed lines show the base sub-lattice to be updated. Thick solid line on the surface shows the y cross-section as a reminder for the one-dimensional roof-top model. When the shown desorption/absorption steps are executed simultaneously they realize a surface diffusion jump of distance $s = 3$ along the y axis.

surface scaling numerically. In particular we have shown that for the $\lambda = 0$ case our simulation results agree with those of the exactly known EW class.

Surface diffusion is a much studied basic process [20]. Several atomistic models have been constructed and investigated with the aim of realizing Mullins-Herring (MH) diffusion [21, 22] and scaling (for a recent review see [23]). The Langevin equation of MH diffusion is a linear one, with a ∇^4 lowest order gradient term

$$\partial_t h(\mathbf{x}, t) = -\kappa \nabla^4 h(\mathbf{x}, t) + \eta(\mathbf{x}, t) . \quad (4)$$

resulting from a curvature driven surface current. This equation is exactly solvable and exhibits scale invariance of the roughness. In Sect. 1.2 we show how this can be realized using the octahedron model.

1.1. The simulations

Dynamic, bit-coded simulations were run on conserved lattice gas models of sizes $L \times L$ following the rule (3). The surface heights were reconstructed from the slopes

$$h_{i,j} = \sum_{l=1}^i \sigma_x(l, 1) + \sum_{k=1}^j \sigma_y(i, k) . \quad (5)$$

The interface width defined as

$$w(L, t) = \left[\frac{1}{L^2} \sum_{i,j}^L h_{i,j}^2(t) - \left(\frac{1}{L^2} \sum_{i,j}^L h_{i,j}(t) \right)^2 \right]^{1/2} \quad (6)$$

has been calculated at certain sampling times t . In the absence of any characteristic length, growth processes are expected to follow a power-law behavior and the average surface width $W = \overline{w}$ can be described by the *Family-Vicsek* [24] scaling law:

$$W(L, t) \simeq L^\alpha f(t/L^z), \quad (7)$$

with the universal scaling function $f(u)$ of the form:

$$f(u) \sim \begin{cases} u^\beta & \text{if } u \ll 1 \\ \text{const.} & \text{if } u \gg 1 \end{cases} \quad (8)$$

Here α is the roughness exponent of the stationary regime, when the correlation length has exceeded the system size L and β is the growth exponent, describing the intermediate time behavior. The dynamical exponent z is the ratio

$$z = \alpha / \beta. \quad (9)$$

For the 2d KPZ universality class our numerical results [18]

$$\alpha = 0.39(1), \quad \beta = 0.245(5), \quad z = 1.6(1) \quad (10)$$

are in agreement with most of the literature values [25, 26]. The MH class, with non-conservative noise is characterized by the exponents

$$\alpha = 1, \quad \beta = 1/4, \quad z = 4 \quad (11)$$

in two dimensions, while in case of conservative (diffusive) noise the exponents are

$$\alpha = 0, \quad \beta = 0, \quad z = 4 \quad (12)$$

and the growth can be logarithmic [7]. Note that in both cases the dynamics is very slow, described by the large dynamical exponent $z = 4$, which makes the simulations time consuming.

Emerging patterns can be characterized by the time dependent power spectrum density (PSD) of the interface

$$S(\mathbf{k}, t) = \langle h(\mathbf{k}, t) h(-\mathbf{k}, t) \rangle, \quad (13)$$

where the height in the Fourier space is computed as

$$h(\mathbf{k}, t) = \frac{1}{L^{d/2}} \sum_{\chi} [h(\chi, t) - \bar{h}] \exp(i\mathbf{k}\chi). \quad (14)$$

We computed $h(\mathbf{k}, t)$ from the surface profiles with the FFT method and determined $S(\mathbf{k}, t)$ by averaging over x and y directions in case of isotropic patterns and only over the direction perpendicular to the ripples in case of x/y anisotropy. We have also calculated the characteristic wavelength of the patterns from the maxima of $S(\mathbf{k}, t)$.

The simulations were started from a flat surface, corresponding to a zig-zag configuration (alternating '1' and '0' lines of the lattice gas) of the slopes (see Fig.1) with periodic boundary conditions. In the model each lattice site can be characterized by 16 different local slope configurations, but we update them only when condition (3) is satisfied. Furthermore, due to the surface continuity, two slopes become redundant, when considering the neighbors. Thus we can describe a lattice site by using only two bits. This permits efficient storage management and large system sizes L . The updates can be performed by bit operations either on multiple samples at once or on multiple sites in parallel. Our multi-sample algorithm proved to be ~ 40 times faster than the conventional FORTRAN 90 code, while a speedup factor of ~ 240 was measured using the multi-site CUDA code on a NVIDIA C2070 graphics card in comparison with a single I5 CPU core running on 2.8 GHz. The latter results could be achieved on huge system sizes up to $L = 2^{17}$. More details are published elsewhere [17, 27, 28].

1.2. Generalizations of the octahedron model

An obvious first step of generalization is to combine the deposition and the removal processes, creating a conserved dynamics. A simultaneous octahedron detachment and deposition in the neighborhood can realize an elementary diffusion step (see Fig. 1). In [29] we described RSOS models with $\Delta h = \pm 1$ height restriction, which in the limit of weak external noise exhibit MH scaling. Microscopic models realizing this behavior are mainly unrestricted solid on solid (SOS) type, which can provide steep slopes and strong curvatures. However, it turned out that the asymptotic universality class of the various limited mobility growth models is a surprisingly subtle issue and some earlier findings proved to be incorrect due to pathologically slow crossover and extremely long transient effects.

In our model the target site is chosen in the $\pm x$ or $\pm y$ direction, with the probabilities: D_{+x} , D_{-x} or D_{+y} , D_{-y} respectively (see Fig.1), thus we can follow **anisotropic surface diffusion** in principle.

Throughout of our studies we normalized the attempt probabilities. The maximal jump distance was fixed to be $s_m \leq 4$ lattice units following computer experiments. To control the surface diffusion

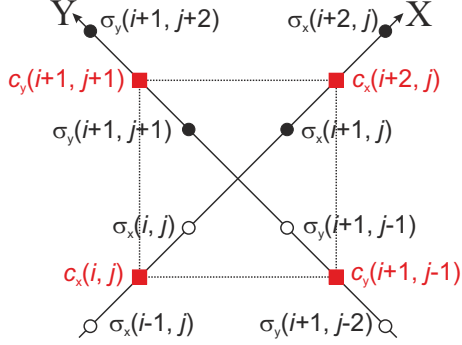


Figure 2: Local slope $\sigma_\chi(i, j)$ (circles) and curvature $c_\chi(i, j)$ (squares) variables at an update site. Filled circles correspond to upward, empty ones to downward slopes of the surface. This plaquette configuration models a valley bottom site.

we imposed additional constraints for the accepting a move. We have tried two kinds of rules based on the local neighborhood configurations. The first one requires that the height of a particle at the final state is higher than that of its initial site

$$h_{\text{fin}} - h_{\text{ini}} \geq 0, \quad (15)$$

which makes the surface more rough (inverse or roughening diffusion). For details of this so-called Larger Height Octahedron Model (LHOD) see [29]. Note, that LHOD introduces up-down anisotropy, which leads to a $\nabla^2[\nabla(h)^2]$ type of nonlinearity and Molecular Beam Epitaxy (MBE) class scaling [29] in general.

The second one is the so-called Larger Curvature Octahedron Model (LCOD), which satisfies the detailed balance condition (1), enabling us to realize linear, equilibrium MH diffusion steps. The local curvature of the surface is calculated at the 4 edges of squares of the projected octahedra as shown on Fig. 2. We followed the scaling behavior of our LCOD in case of smoothing reactions, corresponding to $\kappa > 0$ in Eq. 4. Due to the purely diffusive noise the growth dynamics is logarithmically slow and we find the emergence of the class (12) scaling (see Figure 3).

If the accepted move increases the local curvature, we call it inverse MH (iMH) process. In the continuum model this should correspond to $\kappa < 0$,

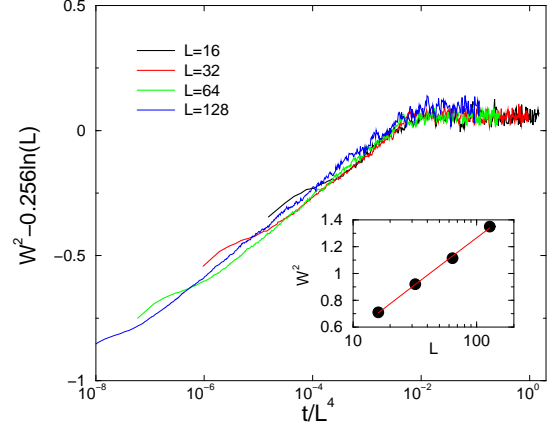


Figure 3: Scaling behavior of the isotropic LCOD model for $L = 16, 32, 64, 128$ (top to bottom at the left side). The data collapse ($f(u)$) has been achieved with the MH class exponents with conservative noise(12). The insert shows the finite size (logarithmic) scaling in the steady state.

an unstable growth, however in the finite, lattice model formation of pyramid-like structures occurs similarly as in the " $n = 2$ " SOS model [30]. When we simulated the evolution of the iMH process (LCOD model) in the presence of a small, competing EW type of noise ($p = q = 0.05$) starting from flat initial condition we found a scaling behavior, which agrees well with that of MH universality class (11) (see Fig. 4). The effective growth exponent defined as

$$\beta_{\text{eff}}(t) = \frac{\ln W(t, L \rightarrow \infty) - \ln W(t/2, L \rightarrow \infty)}{\ln(t) - \ln(t/2)} \quad (16)$$

converges to $\beta = 0.25(1)$ before reaching the saturation regime.

2. Pattern generation by competing inverse MH and KPZ processes

A further step in generalizing our basic surface models was the combination of different subprocesses, resulting in nonequilibrium system with patterns. For example the mixed application of iMH diffusion steps with KPZ updates can model a noisy Kuramoto-Sivashinsky (KS) type of equation [31, 32, 33], the inverse KS (iKS):

$$\partial_t h = \sigma \nabla^2 h + \kappa \nabla^4 h + \lambda (\nabla h)^2 + \eta. \quad (17)$$

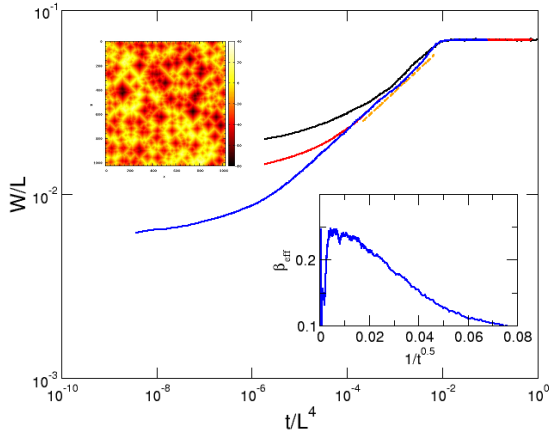


Figure 4: Scaling behavior of the isotropic LCOD model for $L = 32, 64, 128$ (top to bottom at the left side). The data collapse ($f(u)$) has been achieved with the MH class exponents (11). For the growth exponent fitting (dashed line) results in $\beta = 0.25(1)$. The right insert shows the same via the local slopes (16). The left insert is a snapshot of surface heights of the dot patterns generated by the LHOD model with parameters: $D_{\pm x} = D_{\pm y} = 1$ and $p = q = 0.1$ at $t = 10^4$ MCs

However the signs of couplings are reversed with respect to the KS equation¹. This leads to unstable solutions, the long wave behavior of iKS is not defined asymptotically in the continuum model. However, in the lattice regularized version, for intermediate times we expect dynamical scaling of the KS based on symmetry and renormalization arguments [7, 37]. Since the roughening/smoothing surface moves correspond to phase separation/mixing of the lattice gas system it is reasonable to believe that both cases are described by the same universal fixed point behavior.

We performed the surface diffusion steps alternately with the deposition and the removal processes. Thus terms like $\kappa_x \partial^4 h$ and $\kappa_y \partial^4 h$ with $\kappa_x \neq \kappa_y$ can be modeled. We followed the surface roughness and calculated PSD as well as the wavelength growth of the pattern formation.

In case of an anisotropic LHOD a competing EW process always generates stable ripple patterns, but if strong up-down anisotropy (KPZ instead of EW) is applied for late times the ripples become un-

¹Where both the ∇^2 and the ∇^4 terms have negative coefficients and a positive $(\nabla h)^2$ can stabilize the solution.

even, blurred and cut into smaller pieces. If we

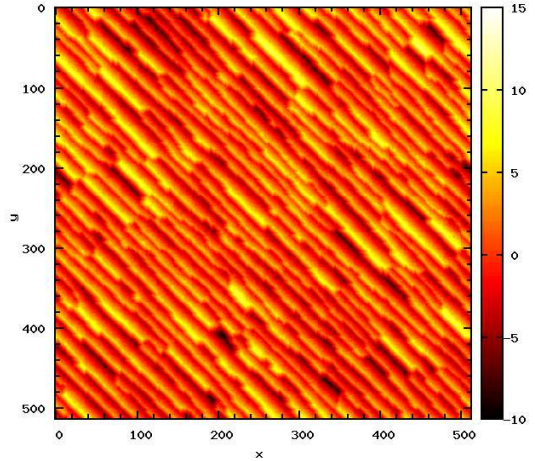


Figure 5: Snapshot of surface heights of the ripple patterns generated by the parameters $D_x = D_y = 0$, $D_{-x} = D_{-y} = 1$ (anisotropic, iMH) and $p = q = 0.05$ adsorption/desorption at $t = 10^4$ MCs, in the LHOD model of linear size $L = 512$.

introduce x/y lattice anisotropy, for example by: $D_x = D_y = 0$ and $D_{-x} = D_{-y} = 1$ the competing weak EW or KPZ moves result in **ripple coarsening** (see Fig. 5), with a wavelength growth $\lambda \propto t^{0.19(1)}$. We calculated this behavior from the maxima of the PSD functions. However, for late times this coarsening slows down for LCOD ($\lambda \propto t^{0.12(1)}$) or becomes faster in case of nonlinear LHOD ($\lambda \propto t^{0.35(5)}$) as shown on Fig. 6. The last value agrees with that of the numerical estimates obtained for the two-field model [38].

When isotropic, iMH competes with a weak EW process one can observe dot formation in both the LHOD and LCOD model. Again, for strong particle deposition or removal the patterns fade away for long times and the KPZ scaling emerges. The insert of Fig. 4 shows a snapshot of the **growing dots** in the LHOD model in the presence of weak EW processes. We have determined the PSDs at different times for $L = 1024$ and deduced the time dependence of the characteristic wavelength from the maxima of $S(\mathbf{k}, t)$ (see Fig. 7).

Having confirmed that the LCOD model exhibits MH class scaling, we introduced a model for the iKS equation (17) as the combination of iMH and KPZ moves. In [29] we presented extensive simulations providing numerical evidence for an asymptotic KPZ scaling of this model. Note, that unlike

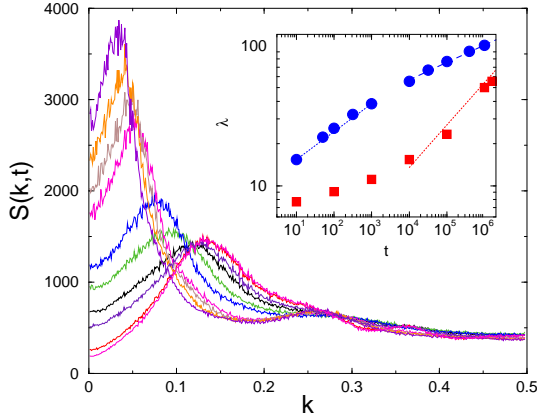


Figure 6: PSD for anisotropic diffusion with $D_y = 1$, $p = q = 0.005$ for $L = 1024$ at different times. The insert shows the wavelength coarsening calculated from the maxima of the PSD curves. Squares: LHOD model with fastening ripple formation $\lambda \propto t^{0.35(5)}$, circles: LCOD model with $p = q = 0$. The lines correspond to power-law fits: $\lambda \propto t^{0.19(1)}$ initially and $\lambda \propto t^{0.12(1)}$ for late times.

the KS, the iKS equation exhibits unstable wavelength amplification. This can be derived in the Fourier space by a linear stability analysis. However the dynamical scaling behavior of the lattice model corresponding to the iKS equation may be expected to be the same as that of the KS equation by symmetry arguments.

3. Conclusions and outlook

We have returned to some unresolved questions of basic surface growth phenomena using mappings and extensive computer simulations. Contrary to many earlier studies we were able to perform numerical analysis in $2 + 1$ dimensions due to the efficient binary lattice gas representation. An important advantage of our method as compared to the analytical approaches is that we can describe anisotropic surface diffusion terms $\kappa_x \partial^4 h$, $\kappa_y \partial^4 h$ by our model.

We have shown that in the zero external noise limit RSOS models can be constructed with short range interactions exhibiting MBE or MH type of surface growth behavior. For inverse (roughening) diffusion, which increases the unstable growth of local curvatures, pyramid-like structures can emerge. The size of these structures is limited only by L , which is not directly comparable with experiments. We created these microscopic models in order to

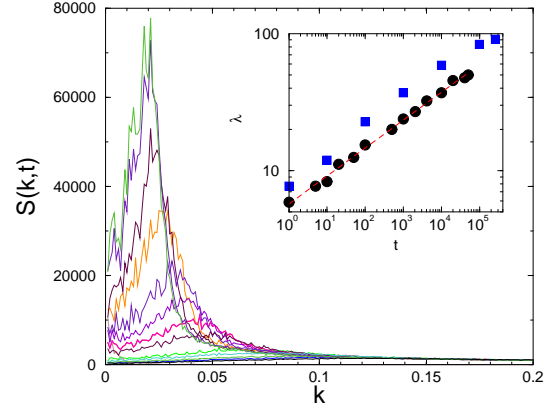


Figure 7: PSD in the LCOD model for isotropic surface diffusion ($D_{\pm x} = D_{\pm y} = 1$) with competing EW moves: $p = q = 0.005$ at different times. The insert shows the wavelength coarsening calculated from the maxima of the PSD curves. Circles correspond to the peaks of the PSD curves, dashed line: power-law fit $\lambda \propto t^{0.20(1)}$. The boxes show the same for $p = q = 0$ in the LCOD. For late times the slope of $\lambda(t)$ decreases.

study them in competition with the non-conserved KPZ processes.

By mapping surface models onto lattice gases, our results imply that the scaling behavior of the oriented diffusion of dimers (KPZ) is stable against the introduction of an attracting force among them. However, a strong repulsion force destroys the fluctuations, resulting in mean-field class behavior [29]. We found numerical evidence, by surface scaling and probability distribution studies, that the iKS model exhibits KPZ scaling in $2 + 1$ dimensions. The construction of a KS model within the framework of the lattice gas mapping is under way. Further studies with different boundary conditions can reveal interesting connections of the surface tilt to the particle concentration of the lattice gas. We emphasize that results for disorder dependence or anomalous diffusion [36] can easily be transformed between these surface and lattice gas models. Extension of our mapping can also help to solve more detailed models of ion-beam induced pattern formation [35, 34], describing the observed narrow band of unstable wave-lengths or hexagonal dot formation [1].

We have also determined the time dependent power spectrum and deduced the wavelength growth of the patterns. We have investigated this for LHOD and LCOD process, with and without

spatial anisotropies. In case of uniaxial surface diffusion ripple morphologies have been found, while for x/y lattice isotropy dot like pattern formation could be traced. The wavelength growth is slow for LCOD models. Usually we found a $\lambda(t) \propto t^{0.19(1)}$ time dependence, which slows down further at late times for the linear LCOD model, but becomes faster in the nonlinear LHOD model. This agrees with the two-field model results [38]. In [29] we estimated the characteristic length scale by a different measure, the average length of the longest slopes. The growth of that scale was found to be even slower, except when steady DC current flowed through the system. Since that quantity measures an extremal property of the patterns one can understand that somewhat different results arise from those of the PSD analysis.

Finally we point out that these models enable efficient, bit-coded, stochastic cellular automaton type of simulation of surfaces which can be run extremely fast on advanced graphic cards [27, 28].

Acknowledgments:

Support from the Hungarian research fund OTKA (Grant No. T77629), the bilateral German-Hungarian exchange program DAAD-MÖB (50450744, P-MÖB/854) is acknowledged. The authors thank the access to the HUNGRID and NVIDIA for supporting the project with high-performance graphics cards within the framework of Professor Partnership.

References

- [1] S. Facsko, T. Dekorsy, C. Koerdt, C. Trappe, H. Kurz, A. Vogt, and H. L. Hartnagel, *Science* **285**, 1551 (1999).
- [2] B. Schmittman and R. K. P. Zia, in *Phase transitions and Critical Phenomena*, edited by C. Domb and J. L. Lebowitz (Academic Press, London, 1996), vol. 17.
- [3] G. Ódor, *Rev. Mod. Phys.* **76**, 663 (2004).
- [4] Z. Rácz, M. Siegert, D. Liu, and M. Plischke, *Phys. Rev. A* **43**, 5275 (1990).
- [5] J. Krug, *Phys. Rev. Lett.* **70**, 3271 (1993).
- [6] R. M. Bradley and J. Harper, *J. Vac. Sci. Tech. A* **6**, 2390 (1988).
- [7] A. L. Barabási and H. E. Stanley, *Fractal Concepts in Surface Growth* (Cambridge University Press, Cambridge, 1995).
- [8] M. Makeev, R. Cuerno, and A.-L. Barabási, *Nucl. Inst. and Meth. B* **197**, 185 (2002).
- [9] M. Kardar, G. Parisi, and Y. Zhang, *Phys. Rev. Lett.* **56**, 889 (1986).
- [10] M. Kardar, *Nucl. Phys. B* **290**, 582 (1987).
- [11] S. F. Edwards and D. R. Wilkinson, *Proc. R. Soc.* **381**, 17 (1982).
- [12] H. Hinrichsen and G. Ódor, *Phys. Rev. Lett.* **82**, 1205 (1999).
- [13] G. Ódor, *Universality In Nonequilibrium Lattice Systems* (World Scientific, 2008).
- [14] H. Rost, *Z. Wahrsch. Verw. Gebiete* **58**, 41 (1981).
- [15] M. Plischke, Z. Rácz, and D. Liu, *Phys. Rev. B* **35**, 3485 (1987).
- [16] P. Meakin, P. Ramanlal, L. Sander, and R. Ball, *Phys. Rev. A* **34**, 5091 (1986).
- [17] G. Ódor, B. Liedke, and K.-H. Heinig, *Phys. Rev. E* **79**, 021125 (2009).
- [18] G. Ódor, B. Liedke, and K.-H. Heinig, *Phys. Rev. E* **81**, 031112 (2010).
- [19] J. Marro and R. Dickman, *Nonequilibrium phase transitions in lattice models* (Cambridge University Press, Cambridge, 1999).
- [20] J. Krug, *Adv. Phys.* **46**, 139 (1997).
- [21] C. Herring, *J. Appl. Phys.* **21**, 301 (1950).
- [22] W. W. Mullins, *J. Appl. Phys.* **28**, 333 (1957).
- [23] M. Constantin and et al., *Phys. Rev. E* **69**, 061608 (2004).
- [24] F. Family and T. Vicsek, *J. Phys. A* **18**, L75 (1985).
- [25] E. Marinari, A. Pagnani, and G. Parisi, *J. Phys. A* **33**, 8181 (2000).
- [26] F. D. A. A. Reis, *Phys. Rev. E* **69**, 021610 (2004).
- [27] Henrik Schulz, Géza Ódor, Gergely Ódor, and Máté. F. Nagy, *Comp. Phys. Comm* **182**, 1476 (2010).
- [28] G. Ódor and J. Kelling (2011), in preparation.
- [29] G. Ódor, B. Liedke, and K.-H. Heinig, *Phys. Rev. E* **81**, 051114 (2010).
- [30] M. Siegert and M. Plischke, *Phys. Rev. E* **50**, 917 (1994).
- [31] Y. Kuramoto and T. Tsuzuki, *Prog. Theor. Phys.* **55**, 356 (1977).
- [32] G. I. Sivashinsky, *Acta Astronaut.* **6**, 569 (1979).
- [33] M. Nicoli, E. Vivo and R. Cuerno, *Phys. Rev. E* **82** (2010) 045202.
- [34] R. Mark Bradley and Patrick D. Shipman, *Phys. Rev. Lett.* **105**, 145501 (2010).
- [35] J. Muñoz-García et al, *Phys. Rev. Lett.* **104**, 026101 (2010).
- [36] M. Nicoli, R. Cuerno, and M. Castro *Phys. Rev. Lett.* **102**, 256102 (2009).
- [37] V. A. Alessandrini, H. J. Vega, and F. Schaposnik, *Phys. Rev. B* **10**, 3906 (1974).
- [38] J. M.-García, R. Cuerno, and M. Castro, *Phys. Rev. B* **78**, 205408 (2008).